Rayleigh-Taylor Growth Stabilization in Direct-Drive Plastic Targets at Laser Intensities of $\sim 1 \times 10^{15}$ W/cm^2

V. A. Smalyuk, S. X. Hu, V. N. Goncharov, D. D. Meyerhofer,* T. C. Sangster, D. Shvarts,† C. Stoeckl, and B. Yaakobi
Laboratory for Laser Energetics, University of Rochester, 250 East River Road Rochester, New York 14623-1299, USA

J. A. Frenje and R. D. Petrasso‡
Plasma Science and Fusion Center, Massachusetts Institute of Technology, Cambridge, Massachusetts 02139, USA
(Received 28 January 2008; published 8 July 2008)

Direct-drive, planar-target Rayleigh-Taylor growth experiments were performed for the first time to test fundamental physics in hydrocodes at peak drive intensities of ignition designs. The unstable modulation growth at a drive intensity of $\sim 1 \times 10^{15}$ W/cm^2 was strongly stabilized compared to the growth at an intensity of $\sim 5 \times 10^{14}$ W/cm^2. The experiments demonstrate that standard simulations based on a local model of electron thermal transport break down at peak intensities of ignition designs (although they work well at lower intensities). The preheating effects by nonlocal electron transport and hot electrons were identified as some of the stabilizing mechanisms.

DOI: 10.1103/PhysRevLett.101.025002 PACS numbers: 52.57.Fg

The goal of inertial confinement fusion (ICF) [1,2] is to implode a spherical target to achieve high compression of the fuel and high temperature of the hot spot to trigger ignition and maximize the thermonuclear energy gain. In a spherical implosion, the target is driven either by direct illumination with overlapped laser beams (direct drive) [1] or by x rays produced in a high-Z enclosure (hohlraum) containing the target (x-ray drive) [2]. The direct-drive-ignition target designs [3] for the National Ignition Facility (NIF) use cryogenic deuterium-tritium shells with outer plastic ablators. The unstable growth of target nonuniformities due to the Rayleigh-Taylor (RT) instability is one the most significant factors disrupting the symmetry of implosions and reducing target compression and fusion yield [1–15]. Experimentally, the hydrodynamic growth of target perturbations has been extensively studied using both x-ray [4,5] and direct [6–9] drive, mostly in planar geometry. Both classical and ablative RT instability linear growth rates have been measured using single-mode perturbations [4–9]. Multimode [10] and broadband [11,12] perturbations were used to measure nonlinear saturation and mode-coupling effects. Experiments in cylindrical [13] and spherical geometry [14,15] were used to measure acceleration-phase and deceleration-phase hydrodynamic growth.

A number of techniques have been developed to reduce initial target nonuniformities seeded by laser imprinting on direct-drive ICF lasers. A combination of distributed phase plates (DPPs) [16], polarization smoothing (PS) [17], and smoothing by spectral dispersion (SSD) [18] is used on the OMEGA laser [19], induced spatial incoherence [20] on the NIKE laser system, and partially coherent light [21] in combination with random-phase plates on the GEKKO-XII laser facility. Targets with foam-buffered layers, high-Z overcoats, and high-Z dopants have been demonstrated to reduce imprinting and RT growth [22–25].

Another source of RT-growth stabilization comes from ablation-front heating caused by electrons from the high-energy tail of the thermal distribution [26–32]. The standard, or local, models of electron transport [33] predict steep gradients of temperature and density near the ablation surface. The nonlocal electrons with energies >10 keV, from the tail of thermal distribution, can penetrate further into the target and cause more preheating than local models, increasing the density scale length and reducing the density at the ablation surface [26–32]. Nonlocal models [26–32] predict significant ablation-front heating when plasma corona temperatures exceed ~ 3 keV. Direct-drive experiments and simulations have shown the importance of these nonlocal effects in green laser-drive experiments [6] even at intensities of $\sim 2 \times 10^{14}$ W/cm^2. Experiments with 351-nm UV light did not show the presence of nonlocal electrons at these low drive intensities [8]. Recent acceleration measurements [31,32] of planar plastic foils showed the importance of nonlocal effects in modeling the laser drive at intensities of $\sim 1 \times 10^{15}$ W/cm^2. This Letter presents the first experimental results where RT growth was measured at NIF-relevant intensities of $\sim 1 \times 10^{15}$ W/cm^2, showing strong RT-growth stabilization compared to local model predictions. These results imply that direct-drive-ignition targets are more stable than previously calculated using local electron-transport models. They show, for the first time, that the standard local model for electron thermal transport breaks down at intensities of $\sim 1 \times 10^{15}$ W/cm^2, requiring nonlocal, hot-electron, and possibly other physics to be included and validated before using them in ignition designs.

In the experiments, 2.5-mm-diam, 20-μm-thick CH targets were driven with 1.6- and 1-ns square pulses on the OMEGA laser system [19]. The targets were driven with up to 14 overlapped beams with full beam smoothing

including DPPs [16], PS [17], and SSD [18]. Target acceleration was measured using side-on radiography with a streak camera and ~2-keV x rays from a dysprosium sidelighter [32]. The RT growth of preimposed 2D modulations was measured with through-foil, x-ray radiography [11] using ~1.3-keV x rays from a uranium backlighter. In the RT experiments, the 2D preimposed modulations had wavelengths of 20, 30, and 60 μm, with initial amplitudes of 0.05, 0.05, and 0.125 μm, respectively. Figure 1(a) shows two laser pulse shapes used in the experiments: a 1.6 ns square at peak laser intensity of $\sim 5 \times 10^{14}$ W/cm^2 and a 1 ns square at peak laser intensity of $\sim 1 \times 10^{15}$ W/cm^2. The measured trajectories for these two experiments are shown in Fig. 1(b). The target acceleration was higher using a 1-ns pulse than with a 1.6-ns pulse due to the higher laser intensity. These trajectory measurements are in very good agreement with predictions of a 2D hydrocode [32] DRACO (solid curves) using the local model for electron thermal transport, showing that the target acceleration was modeled well by these simulations (the acceleration is needed for the analysis of the RT-growth data).

The results of the RT-growth experiments are shown in Fig. 2 for the 1-ns drive [(a)–(c)] and the 1.6-ns drive [(d)–(f)]. The data were measured using through-foil radiography where the backlighter x rays were imaged by an 8-μm pinhole array onto a framing camera, allowing up to eight images with a temporal resolution of ~80 ps and a spatial resolution of ~10 μm to be captured at different times in each shot [11]. The solid lines are the results of the 2D hydrocode [32] DRACO with a local model for electron transport. One-dimensional nonlocal RT-growth predictions [29] are discussed below. The RT-growth rate as a function of modulation wave number k is given by the dispersion relation [34] $\gamma(k) = 0.94[kg/(1 + kL_m)]^{0.5} - 1.5kV_a$, where g is the target acceleration, V_a is the ablation velocity, and L_m is the density scale length. The experimental data at a long wavelength of 60 μm, weakly affected by the stabilizing term $-1.5kV_a$ [Figs. 2(a) and 2(d)], show that modulations grow stronger at a drive intensity of $\sim 1 \times 10^{15}$ W/cm^2 than at $\sim 5 \times 10^{14}$ W/cm^2. This indicates that the acceleration is higher at the higher intensity, consistent with the trajectory results shown in Fig. 1. At this wavelength, the growth rate is dominated by the first term in the dispersion relation, which is proportional to $(kg)^{0.5}$ (assuming that $kL_m \ll 1$, which is typically the case in these experiments). At an intensity of 5×10^{14} W/cm^2, the short-wavelength modulations (at wavelengths of 20 and 30 μm) grow faster than the long, 60-μm-wavelength modulation. At a high intensity of 1×10^{15} W/cm^2, this trend is reversed:

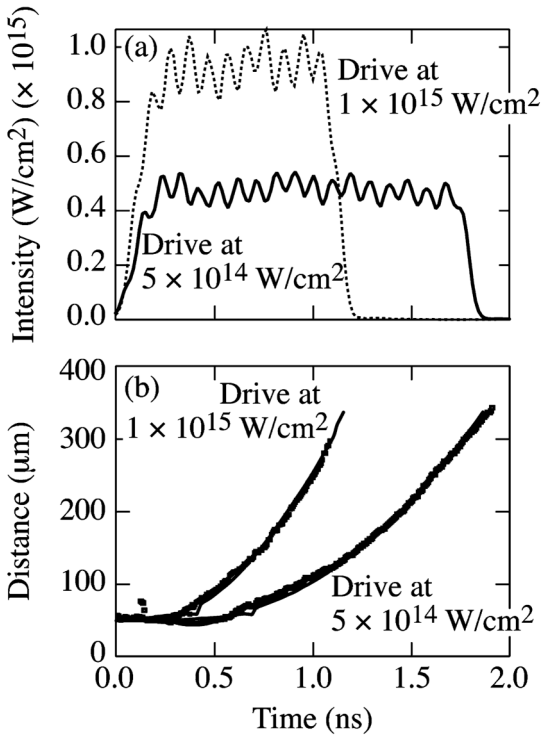

FIG. 1. (a) Intensity vs time for laser drives at intensities of $\sim 5 \times 10^{14}$ and $\sim 1 \times 10^{15}$ W/cm^2. (b) Measured and simulated (smooth curves) planar-target trajectories with drives at $\sim 5 \times 10^{14}$ and $\sim 1 \times 10^{15}$ W/cm^2.

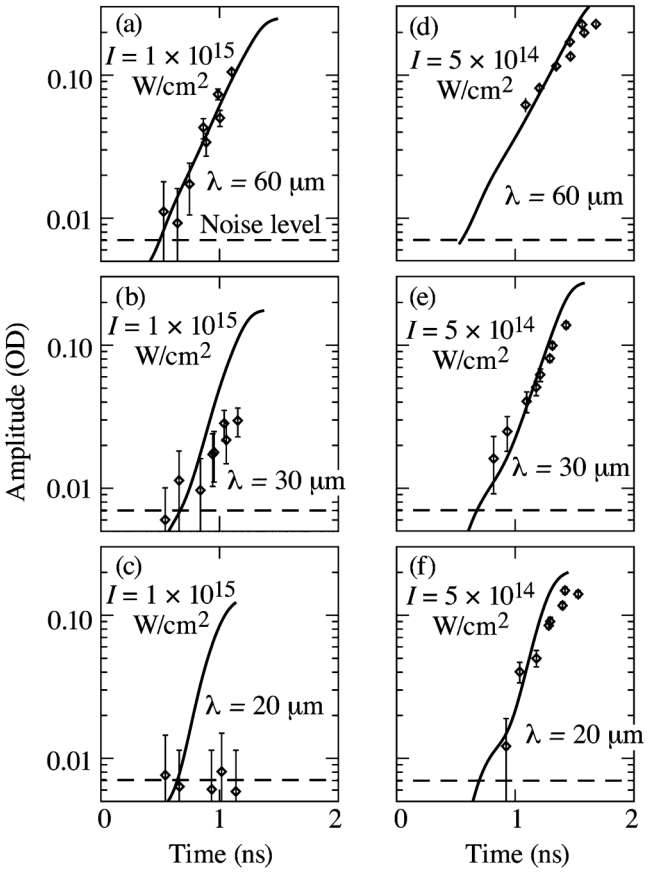

FIG. 2. Optical-depth modulations vs time for drives at intensities of (a)–(c) $\sim 1 \times 10^{15}$ W/cm^2 and (d)–(f) $\sim 5 \times 10^{14}$ W/cm^2 with wavelengths of (c),(f) 20 μm, (b),(e) 30 μm, and (a),(d) 60 μm. Results of 2D DRACO simulations are shown by solid curves.

60-μm-wavelength modulation grows faster than the 30-μm perturbation, with the 20-μm-wavelength perturbation completely stabilized. Simulation predictions based on the local model show faster growth at shorter wavelengths compared to longer wavelengths at both intensities. The measured stabilization of the short-wavelength modulations at a drive intensity of $\sim 1 \times 10^{15}$ W/cm^2 is consistent with a higher value of the stabilizing term in the dispersion relation. The experiments demonstrate, for the first time, that standard simulations based on a local model of electron thermal transport break down at peak intensities of ignition designs, although they work well at lower intensities. This is the result of critical importance to direct-drive ICF. Another critical result is that the measured strong RT-growth stabilization will alleviate requirements for the mitigation of the hydroinstability growth in direct-drive ignition capsules on NIF, the area of intensive research. The discussion below identifies some of the physics that needs to be included into hydrocodes before they can be reliably used in ignition designs.

Because the ablation velocity is inversely proportional to the density at the unstable ablation surface, the experimental data suggest that the ablation surface has been preheated during the high-intensity drive, leading to decompression. Since the experimental data agree reasonably well with simulations at the drive intensity of $\sim 5 \times 10^{14}$ W/cm^2, the decompression becomes important only at high intensities. Previous experiments [8] at an even-lower intensity of $\sim 2 \times 10^{14}$ W/cm^2 agreed well with 2D simulations, indicating no decompression at low intensities. The nonlocal electron transport is one of the candidates responsible for the preheat. Preheat by nonlocal thermal electrons was shown to stabilize the RT growth in targets driven by green lasers even at low intensities of $\sim 1 \times 10^{14}$ W/cm^2 [4,6,9]. In addition, the target preheat from hot electrons generated by two-plasmon-decay (TPD) instability could also be responsible for observed growth stabilization [35,36].

Figure 3(a) shows a measured [37] hard-x-ray signal (with photon energies $>$40 keV) along with the drive history at a drive intensity of $\sim 1 \times 10^{15}$ W/cm^2. The hard-x-ray signal is present at the last $\sim$500 ps of the drive, when the RT-growth data were collected. The measured temperature of hot electrons [37] (inferred from the hard-x-ray spectrum) was $\sim$60 keV, indicating that the whole target can be uniformly heated by hot electrons because the stopping range of the $\sim$60-keV electron is larger than the target thickness during the time when electrons are produced. As hot electrons leave the target, they charge it; as a result, ions follow them, accelerating to high energies of up to a few MeV [38]. Figure 3(b) shows the measured ablator-proton [38] (associated with the presence of hot electrons) spectrum, showing the proton energy cutoff at $\sim$0.5 MeV, corresponding to a hot-electron temperature of $\sim$55 keV [39], consistent with hard-x-ray measurements. Target preheat at the end of the drive is estimated (based on a model from Ref. [36]) to be in the range of 8 ± 5 eV

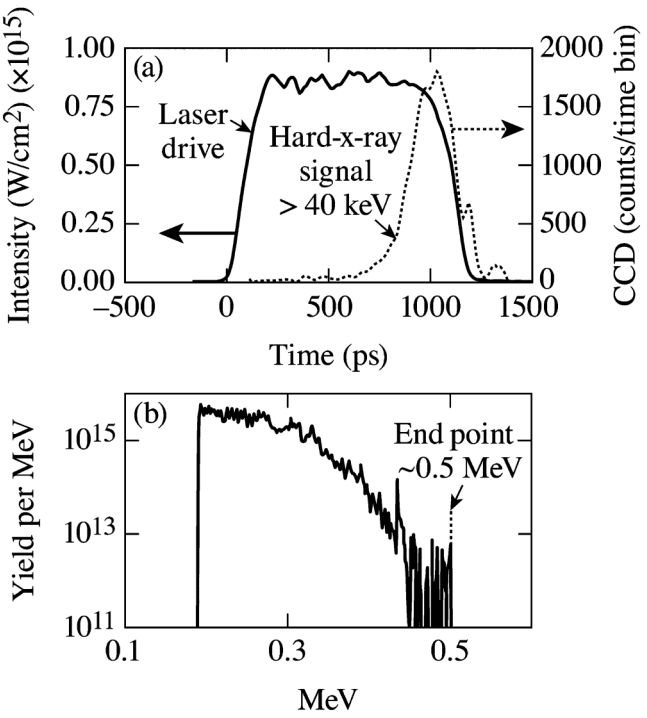

FIG. 3. (a) Intensity vs time (solid curve) and hard-x-ray signal vs time (dotted curve) for a drive intensity of $\sim 1 \times 10^{15}$ W/cm^2. (b) Ablator-proton spectrum for the drive at $\sim 1 \times 10^{15}$ W/cm^2.

(target temperature simulated by a local model was 45 eV). This corresponds to a range of density reduction of (18 ± 9)%, based on 1D simulations. Figure 4 shows growth rates as a function of spatial wavelength calculated by the 1D code LILAC for an intensity of $\sim 1 \times 10^{15}$ W/cm^2 using (1) the local electron transport (solid curve), (2) the local electron transport including effects of hot-electron preheat (dashed curve), and (3) nonlocal electron transport [29] (dotted curve). In nonlocal calculations at an intensity of $\sim 1 \times 10^{15}$ W/cm^2, the ablation velocity was $\sim$20% higher than the local, and the density scale length was $\sim$50% larger. To account for hot-electron preheat, the ablation velocity and density scale length were increased by 18% compared to local predictions. A calculation using the local model shows the trend shown by 2D simulations with shorter wavelengths having faster growth rates than longer wavelengths. This trend is still present if hot-electron preheat is added in the local calculations. The nonlocal calculation shows a trend more consistent with the experiments, modulations at 30-μm wavelength having less growth than 60-μm-wavelength modulations and the growth of 20-μm-wavelength modulation completely stabilized. The ablation-front preheat due to nonlocal electrons is beneficial for ICF targets unless it extends through the whole target (as in the case of hot electrons). In this case, the target cannot be efficiently compressed, resulting in a degradation of its performance [40].

While the observed RT-growth stabilization correlates with a presence of nonlocal and hot electrons, the radiation

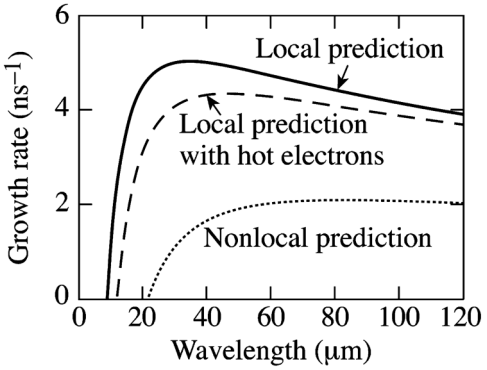

FIG. 4. One-dimensional predictions of the RT-growth rate as a function of spatial frequency using a local electron-transport model (solid curve), a local model with hot-electron preheat (dashed curve), and a nonlocal model (dotted curve) at an intensity of $\sim 1 \times 10^{15}$ W/cm^2.

preheat was also considered as a source of stabilization. Previous x-ray measurements [41] in solid plastic spheres showed a good agreement between measured and simulated x-ray production in the broad spectral range of x rays from 0.2 to 5 keV. Therefore, radiation preheat is an unlikely source of observed RT-growth stabilization at high intensities.

In conclusion, direct-drive, Rayleigh-Taylor growth experiments were performed on the OMEGA laser facility using planar plastic targets at NIF-relevant intensities. The unstable modulation growth at a drive intensity of $\sim 1 \times 10^{15}$ W/cm^2 was strongly stabilized relative to the growth at an intensity of $\sim 5 \times 10^{14}$ W/cm^2. This shows that the standard local model for electron thermal transport breaks down at intensities of $\sim 1 \times 10^{15}$ W/cm^2. The measured growth reduction correlates with the presence of a preheat due to nonlocal electrons and hot electrons generated by the TPD instability. As a result, the nonlocal, hot-electron, and possibly other physics needs to be included into hydrocodes and validated before using them in ignition designs. The measured strong RT-growth stabilization will alleviate requirements for the mitigation of the hydroinstability growth in direct-drive ignition capsules on NIF.

This work was supported by the U.S. Department of Energy Office of Inertial Confinement Fusion under Cooperative Agreement No. DE-FC52-08NA28302, the University of Rochester, and the New York State Energy Research and Development Authority. The support of DOE does not constitute an endorsement by DOE of the views expressed in this article.

*Also Departments of Mechanical Engineering and Physics & Astronomy.
†Also at Nuclear Research Center, Negev, Israel.
‡Visiting senior scientist from Laboratory for Laser Energetics.

[1] S. Atzeni and J. Meyer-ter-Vehn, *The Physics of Inertial Fusion: Beam Plasma Interaction, Hydrodynamics, Hot Dense Matter*, International Series of Monographs on Physics (Clarendon Press, Oxford, 2004).
[2] J. D. Lindl, *Inertial Confinement Fusion: The Quest for Ignition and Energy Gain Using Indirect Drive* (Springer-Verlag, New York, 1998).
[3] P. W. McKenty *et al.*, Phys. Plasmas **8**, 2315 (2001).
[4] S. G. Glendinning *et al.*, Phys. Rev. Lett. **78**, 3318 (1997).
[5] B. A. Remington *et al.*, Phys. Rev. Lett. **73**, 545 (1994).
[6] K. Shigemori *et al.*, Phys. Rev. Lett. **78**, 250 (1997).
[7] C. J. Pawley *et al.*, Phys. Plasmas **6**, 565 (1999).
[8] J. P. Knauer *et al.*, Phys. Plasmas **7**, 338 (2000).
[9] H. Azechi *et al.*, Phys. Rev. Lett. **98**, 045002 (2007).
[10] M. M. Marinak *et al.*, Phys. Rev. Lett. **80**, 4426 (1998).
[11] V. A. Smalyuk *et al.*, Phys. Rev. Lett. **95**, 215001 (2005).
[12] V. A. Smalyuk *et al.*, Phys. Plasmas **13**, 056312 (2006).
[13] D. L. Tubbs *et al.*, Phys. Plasmas **6**, 2095 (1999).
[14] C. Cherfils *et al.*, Phys. Rev. Lett. **83**, 5507 (1999).
[15] V. A. Smalyuk *et al.*, Phys. Rev. Lett. **87**, 155002 (2001).
[16] Y. Lin, T. J. Kessler, and G. N. Lawrence, Opt. Lett. **20**, 764 (1995).
[17] T. R. Boehly *et al.*, J. Appl. Phys. **85**, 3444 (1999).
[18] S. P. Regan *et al.*, J. Opt. Soc. Am. B **17**, 1483 (2000).
[19] T. R. Boehly *et al.*, Opt. Commun. **133**, 495 (1997).
[20] R. H. Lehmberg and S. P. Obenschain, Opt. Commun. **46**, 27 (1983).
[21] H. Nakano *et al.*, J. Appl. Phys. **73**, 2122 (1993).
[22] H. Azechi *et al.*, Phys. Plasmas **4**, 4079 (1997).
[23] R. G. Watt *et al.*, Phys. Rev. Lett. **81**, 4644 (1998).
[24] M. Nakai *et al.*, Phys. Plasmas **9**, 1734 (2002).
[25] S. P. Obenschain *et al.*, Phys. Plasmas **9**, 2234 (2002).
[26] A. R. Bell, R. G. Evans, and D. J. Nicholas, Phys. Rev. Lett. **46**, 243 (1981).
[27] E. M. Epperlein and R. W. Short, Phys. Fluids B **3**, 3092 (1991).
[28] A. Sunahara *et al.*, Phys. Rev. Lett. **91**, 095003 (2003).
[29] V. N. Goncharov *et al.*, Phys. Plasmas **13**, 012702 (2006).
[30] W. Manheimer and D. Colombant, Phys. Plasmas **11**, 260 (2004).
[31] G. Schurtz *et al.*, Phys. Rev. Lett. **98**, 095002 (2007).
[32] S. X. Hu *et al.*, "Validating Thermal Transport Modeling with Planar-Foil Experiments on OMEGA" (to be published).
[33] R. C. Malone, R. L. McCrory, and R. L. Morse, Phys. Rev. Lett. **34**, 721 (1975).
[34] R. Betti *et al.*, Phys. Plasmas **5**, 1446 (1998).
[35] W. L. Kruer, in *The Physics of Laser-Plasma Interactions, Frontiers in Physics*, edited by D. Pines (Addison-Wesley, Redwood City, CA, 1988), Vol. 73.
[36] B. Yaakobi *et al.*, Phys. Plasmas **12**, 062703 (2005).
[37] C. Stoeckl *et al.*, Phys. Rev. Lett. **90**, 235002 (2003).
[38] D. G. Hicks *et al.*, Phys. Plasmas **8**, 606 (2001).
[39] J. A. Frenje, MIT (private communication).
[40] V. A. Smalyuk *et al.*, Phys. Rev. Lett. **100**, 185005 (2008).
[41] S. P. Regan *et al.*, Bull. Am. Phys. Soc. **51**, 254 (2006).